AGU Advances

RESEARCH ARTICLE
10.1029/2021AV000475

Seismic Detection of Oceanic Internal Gravity Waves From Subaerial Seismometers

Heather R. Shaddox[1], Emily E. Brodsky[1], Steven R. Ramp[2], and Kristen A. Davis[3]

[1]Department of Earth and Planetary Sciences, University of California, Santa Cruz, Santa Cruz, CA, USA, [2]Soliton Ocean Services, LLC, Falmouth, MA, USA, [3]Department of Civil and Environmental Engineering and Earth System Science, University of California, Irvine, Irvine, CA, USA

Key Points:

- Internal waves can generate local tilt potentially observable on subaerial broadband seismometers
- We find promising evidence of the first onshore seismic detection of internal waves
- Seismic coupling preferentially selects waves that collide nearshore

Supporting Information:

Supporting Information may be found in the online version of this article.

Correspondence to:

H. R. Shaddox,
hshaddox@ucsc.edu

Citation:

Shaddox, H. R., Brodsky, E. E., Ramp, S. R., & Davis, K. A. (2021). Seismic detection of oceanic internal gravity waves from subaerial seismometers. *AGU Advances*, *2*, e2021AV000475. https://doi.org/10.1029/2021AV000475

Received 26 APR 2021
Accepted 26 JUL 2021

Peer Review The peer review history for this article is available as a PDF in the Supporting Information.

Abstract Oceanic internal gravity waves propagate along density stratification within the water column and are ubiquitous. They can propagate thousands of kilometers before breaking in shoaling bathymetry and the ensuing turbulent mixing affects coastal processes and climate feedbacks. Despite their importance, internal waves are intrinsically difficult to detect as they result in only minor amplitude deflection of the sea surface; the need for global detection and long time series of internal waves motivates a search for geophysical detection methods. The pressure coupling of a propagating internal wave with the sloping seafloor provides a potential mechanism to generate seismically observable signals. We use data from the South China Sea where exceptional oceanographic and satellite time series are available for comparison to identify internal wave signals in an onshore passive seismic data set for the first time. We analyze potential seismic signals on broadband seismometers in the context of corroborating oceanographic and satellite data available near Dongsha Atoll in May–June 2019 and find a promising correlation between transient seismic tilt signals and internal wave arrivals and collisions in oceanic and satellite data. It appears that we have successfully detected oceanic internal waves using a subaerial seismometer. This initial detection suggests that the onshore seismic detection and amplitude determination of oceanic internal waves is possible and can potentially be used to expand the historical record by capitalizing on existing island and coastal seismic stations.

Plain Language Summary Oceanic internal gravity waves are similar to the more familiar surface gravity waves that travel along the air-water density boundary at the surface of the ocean, but instead travel along density boundaries within the water column. Internal waves are important for coastal processes, climate feedbacks, and general oceanic dynamics and are therefore important to detect and track on a global scale over time. However, since internal waves are buried within the water column, they are difficult to detect. Seismology may be able to aid in detecting and measuring the size of internal waves since a traveling internal wave will deform the underlying seafloor and generate a local tilt signal that should be observable on coastal broadband seismometers. Here we perform an initial evaluation of the seismic detectability of internal waves by using Dongsha Atoll in the South China Sea where we compare an onshore broadband seismometer to internal waves identified in corroborating oceanic and satellite data. We find correlations between the timing of transient seismic tilt signals and internal waves identified in oceanic and satellite data. This is promising evidence of the first onshore seismic detection of internal waves.

1. Internal Waves and Expected Seismic Signals

Oceanic internal gravity waves propagate along density stratification within the water column (Helfrich & Melville, 2006). These waves are ubiquitous and can propagate thousands of kilometers before breaking on shoaling bathymetry and the ensuing turbulent mixing affects coastal processes, climate feedbacks, and marine ecosystems (DeCarlo et al., 2015; MacKinnon et al., 2017; Reid et al., 2019; Wolanski & Deleersnijder, 1998; Wang et al., 2007). Internal waves are of further importance for submarine navigation, subsurface structures, hydroacoustics, and marine organisms, and their critical role in mixing, energy dissipation, and thermohaline circulation make them one of the most important factors governing oceanic dynamics (Garrett & Kunze, 2007; Ferrari & Wunsch, 2009; Miropol'sky, 2001; Woodson, 2018). Internal waves of tidal frequency, called internal tides or baroclinic tides, are generated in stratified waters when barotropic tidal currents interact with seafloor topography. Internal tides play a particularly important role in oceanic

dynamics because they are generated regularly and transfer energy from tides to mixing both in the deep ocean and on continental shelves (Garrett & Kunze, 2007; Sandstrom & Elliott, 1984). Yet, they are not always generated, even in the same ocean basin. Whether internal tides are generated depends on tide-topography interactions and ocean stratification (Garrett & Kunze, 2007). Seasonal and climatological modifications in density stratification can result in dramatic changes in internal tide generation and propagation. Once generated, internal tides can propagate hundreds of kilometers and then break up into shorter, higher-frequency nonlinear internal waves (Holloway et al., 1997; Ray & Mitchum, 1996; Zhao et al., 2004).

Despite their importance, internal waves are intrinsically difficult to detect from remote sensing approaches as they produce only minor amplitude deflection of the sea surface. Detection of internal waves through sea surface roughness variations visible on satellite images is possible (Alpers, 1985; Jackson et al., 2013) but limited by cloud cover and temporal resolution, which is often greater than a tidal period, making it challenging to create a continuous time series of internal waves. Therefore, short-term (weeks-months) field deployments with in-situ oceanographic measurements of temperature, pressure and currents at appropriate depths are used to successfully detect internal waves. However, these deployments only measure deflections at certain depths and can miss some waves. More importantly, they do not provide basin-scale spatial coverage or long time series records. The need for global detection and long time series of internal waves motivates a search for geophysical detection methods.

The pressure coupling of a propagating internal wave with the seafloor provides a potential mechanism to generate seismically observable signals. It is already well-established that oceanic surface waves generate "noise" on seismometers (Orcutt et al., 1993). There is a ubiquitous seismic noise peak at periods of approximately 2.5–25 s caused by ocean surface wave energy coupling into the ocean bottom, either from ocean waves in shallow water interacting with coastlines (primary microseisms) or wave-wave interactions (secondary microseisms) (Bromirski, 2001; Bromirski et al., 2005; Tanimoto, 2007). Infragravity waves, ocean surface waves with periods longer than swell and wind-driven waves, have generated long period (20–400 s) signals on ocean-bottom seismometers (OBS) (Dolenc et al., 2008). Internal tides have also been recorded by OBS, including at the ocean bottom from "tremor" signals on OBS geophones (Chang et al., 2016) and infrequent (roughly twice per month) internal tidal bores identified as tilt signals on a broadband OBS (Fukao et al., 2016). Breaking internal waves were also potentially detected on a seafloor distributed acoustic sensing cable (Lindsey et al., 2019). It is interesting to note that earthquakes can produce acoustic waves that propagate along the low velocity channel of the ocean (T-waves), and travel times of T-waves are impacted by the internal tide (Munk et al., 1981; Sugioka et al., 2005; Wu et al., 2020). Tsunami waves are a type of infragravity wave that have induced tilt signals due to loading on the seafloor observable on both island (Nishida et al., 2019; Yuan et al., 2005) and coastal (Boudin et al., 2013; Nawa et al., 2007) broadband seismometers; it is therefore possible for seafloor pressure perturbations to generate near-field tilt that is observable onshore.

A typical South China Sea internal solitary wave (i.e., nonlinear dispersive wave) of depression with an amplitude of 100 meters results in a hydrostatic pressure change of approximately 2.5 kPa (Moum & Smyth, 2006), which should generate a near-field tilt on the seafloor around 40 nanoradians (nrad) (see Text S2 for calculation). Broadband seismometers record rotational motion/tilt in addition to translational motion because the gravitational force due to a tilt change results in an acceleration (Wielandt & Forbriger, 1999). A tilt on the order of tens of nrad should be observable at long periods (>100 s) on a broadband seismometer (Ackerley, 2014), and would be expected as internal waves approach and pass a seismic station (Figure 1a). Since the seafloor is elastic, a broadband seismometer can also detect a near-field quasi-static tilt signal from a wave not passing directly over the instrument if the wave is within a distance roughly equal to the finite source length (i.e., the wavelength of the wave), similar to what has been observed on island and coastal seismic stations from passing tsunami waves. This is a simplified view that provides a minimum bound on the potentially observable seismic signals. As will be discussed later in this study, additional pressure sources associated with propagating internal waves would provide additional tilt. For instance, the dynamic pressure change on the seafloor from breaking or interacting internal waves may also result in a seismically observable signal through the same type of elastic interaction illustrated in Figure 1a (Moum & Smyth, 2006). In principle, seismology should be able to fill in the observational gap and provide long-term time series of internal waves.

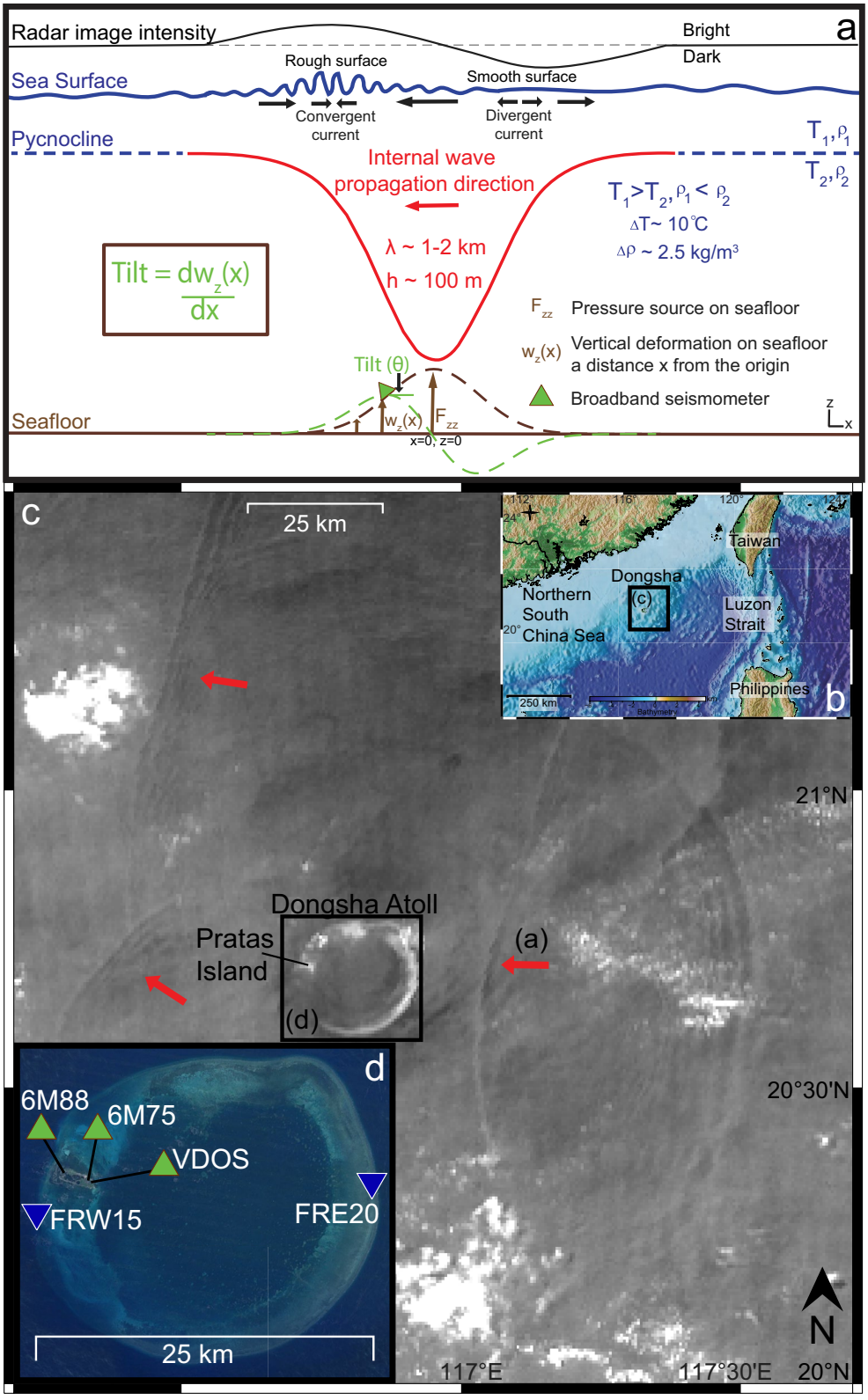
Radar image intensity
Bright
Dark
a
Rough surface
Smooth surface
Sea Surface
Convergent current
Divergent current
Pycnocline
T1,ρ1
T2,ρ2
Internal wave propagation direction
T1>T2, ρ1 < ρ2
ΔT~ 10℃
Δρ ~ 2.5 kg/m3
λ ~ 1-2 km
h ~ 100 m
Tilt = dwz(x)/dx
Fzz Pressure source on seafloor
wz(x) Vertical deformation on seafloor a distance x from the origin
Broadband seismometer
Tilt (θ)
Seafloor
wz(x)
Fzz
x=0, z=0
z
x
c
25 km
Taiwan
Dongsha
Northern South China Sea
(c)
Luzon Strait
Philippines
250 km
b
21°N
Dongsha Atoll
Pratas Island
(d)
(a)
d
6M88
6M75
VDOS
FRW15
FRE20
25 km
20°30'N
N
117°E
117°30'E
20°N

Figure 1.

Previous studies detecting internal tides and possibly internal waves using seismology have been based on sparse ocean-bottom instrumentation with little oceanographic context or corroborating data. Here we perform an initial evaluation of the subaerial seismic detectability of internal waves by analyzing potential seismic signals in the context of corroborating data. This pilot project is possible because of exceptional in situ data available from Dongsha Atoll in the South China Sea. On Pratas Island at the western side of Dongsha Atoll (Figures 1c and 1d) a permanent seismic station (VDOS) and two temporary seismometers (May–June 2019) provide broadband seismic data. A temporary oceanographic deployment (May–June 2019) and available satellite data provide constraints on the arrival times of internal waves at Dongsha Atoll. We find a promising correlation between transient seismic tilt signals and internal wave arrival times in oceanic and satellite data, potentially leading the way to utilizing seismology for both the detection and amplitude determination of internal waves. Further, since there have been roughly 700 operational island stations since the first island station was installed in 1957, the technique applied to global island as well as coastal seismic stations could potentially provide information about the historic record and track the potential reaction of internal waves to climate change.

2. Dongsha Atoll and the South China Sea

The largest amplitude (>100 m) internal solitary waves (i.e., nonlinear dispersive waves) in the world have been observed in the South China Sea. Depending on the stratification, internal solitary waves can propagate as waves of depression or elevation. The pycnocline in the South China Sea is <100 m, but the basin is deep (up to 5,000 m depth). This type of stratification is expected to generate waves of depression as have been observed in the northern South China Sea (Fu et al., 2012; Ramp et al., 2010; Simmons et al., 2011). Large diurnal and semidiurnal barotropic tidal currents flow roughly east-west over two north-south trending ridges in the Luzon Strait (Figure 1b), generating strong internal tides that propagate westward into the South China Sea in a narrow beam, steepening into internal solitary waves of depression (Alford et al., 2015; Duda et al., 2004; Lien et al., 2005; Ramp et al., 2004). Internal solitary waves, typically two per day, are generated at peak tidal velocities and their amplitude is modulated on a fortnightly cycle, with the largest amplitude waves generated at peak spring tide when the barotropic tidal forcing is greatest (Duda et al., 2004; Lien et al., 2005; Ramp et al., 2004). Internal waves occur regularly in the South China Sea between March and November and occasionally from December to February (Simmons et al., 2011). Ocean stratification is strongest in autumn and weakest in winter; since the generation of internal tides is dependent on stratification, this is likely the cause for the significant decrease in internal wave generation in the winter.

Dongsha Atoll is a 28 km diameter coral reef at the edge of the continental shelf in the northern South China Sea located approximately 500 km west of the Luzon Strait (Figure 1). It takes roughly 50 h for internal waves generated in the Luzon Strait to arrive at Dongsha Atoll (Davis et al., 2020). Both modeling and observations of internal solitary waves as they propagate upslope at Dongsha Atoll suggests that an incident symmetric depression wave collapses into a packet of elevation waves during shoaling (Fu et al., 2012; Rogers et al., 2019). These wave trains break into northern and southern arms that refract around the atoll, eventually colliding and then reforming west of Dongsha Atoll (Figure 1c).

3. Data and Methods

In order to identify internal wave signals in passive seismic data, we compare seismic observations from one permanent and two temporary seismic stations onshore of Pratas Island to established internal wave signals in satellite and oceanographic data during a temporary deployment in mid-May to mid-June 2019.

Figure 1. Map of the study area and schematic of a propagating internal solitary wave in the South China Sea. (a) Cartoon of a typical internal solitary wave in the South China Sea and the resulting (exaggerated) transient deformation (dashed brown curve), near-field tilting (dashed green curve) of the underlying seafloor (brown line), sea surface roughness (solid blue line), and radar image intensity (black line). This is a simplified cartoon that does not account for the interaction with the coast or nonlinear wave-wave interactions that would complicate an onshore signal. (b) Bathymetric map of the northern South China Sea. (c) Himawari-8 standard red channel image of sea surface reflections on May 15, 2019 05:30 UTC near Dongsha Atoll. Westward propagating internal waves are indicated by red arrows, including an incoming internal solitary wave from the Luzon Strait 500 km east of Dongsha Atoll, and the northern and southern arms of internal wave trains that are interacting and reforming west of Dongsha Atoll. (d) Zoom in of Dongsha Atoll. Oceanic temperature sensors shown as blue inverted triangles and subaerial broadband seismometers on Pratas Island are shown as green triangles.

3.1. Satellite and Oceanographic Data

Alternating convergence and divergence zones above internal waves result in sea surface roughness changes that are visible from sun glint on satellite images (Alpers, 1985; Jackson et al., 2013). We use the 10-minute temporal and 500-meter spatial resolution standard red channel (0.64 μm wavelength) data of the Himawari-8 geostationary meteorological satellite operated by the Japan Meteorological Agency to identify internal waves based on sea surface roughness changes for comparison to seismic observations (Figures 1a and 1c). With these images we can identify internal waves near Dongsha Atoll during daylight hours when there is little cloud cover.

Shoreward of the 100-meter isobath on Dongsha Atoll, internal solitary waves have transformed into packets of elevation waves (Davis et al., 2020; Fu et al., 2012). This is recorded as a sudden drop in water temperature measurements, approximately 4–8°C within several minutes, and is a well-established indicator of the passage of internal waves (Davis et al., 2020). We can therefore use the arrival times of internal waves from in-situ oceanographic temperature measurements to compare to a potential internal wave signal in coastal seismic data. To this end, we use 1–10 s sampling rate oceanic temperature measurements in the water column and on the ocean bottom during a temporary deployment in May/June 2019 around the fore reef of Dongsha Atoll (Figure 1d). We utilize a 20-meter mooring on the eastern side of Dongsha Atoll (FRE20) at 19 meters depth from May 13–June 11, 2019 and an ocean bottom temperature sensor at approximately 16.8 meters depth on the western side of Dongsha Atoll (FRW15) roughly 4.5 km southwest of a permanent seismic station onshore of Pratas Island from May 19–June 6, 2019. These shallow temperature sensors are located at depths where the large internal waves have already broken down slope into nonlinear elevation waves or internal bores, but they will still capture an internal wave signal, albeit a more complex and high-frequency one and lagged from the arrival time of the wave in deeper water as the wave decelerates in shallow water (Davis et al., 2020). Further, these point measurements may miss internal wave arrivals depending on stratification and reflection properties of the internal waves.

To help guide the detection of internal waves arriving from the Luzon Strait on these two shallow temperature sensors we rely on the timing of internal wave detections from two deeper (300 and 500 m depth) moorings 6–9 km east of Dongsha Atoll before internal solitary waves of depression have interacted much with the bottom or transformed into packets of elevation waves. In particular, we use the wave arrival times at the 300 m mooring, wave velocities calculated between the 500 and 300 m moorings, and the distances from the 300 m mooring to the eastern (FRE20; 6.7 km) and western (FRW15; 30.9 km) sensors to estimate the wave arrival times at these shallow sensors. However, these are used as rough time estimates only since they are based on the wave velocity between the 500 and 300 m moorings, which on average was 1.8 m/s during the deployment, and wave velocities can decrease to below 0.5 m/s in shallow water (Davis et al., 2020; Fu et al., 2012). Variations in wave velocity create uncertainty in arrival times at the shallow temperature sensors. For example, a wave with a phase speed of 2 m/s would propagate around the 28 km diameter atoll in approximately 3.9 h, while a wave with a phase speed of 1 m/s would propagate the same distance in 7.8 h. It is therefore difficult to predict the exact arrival time of waves at the shallow sensors without measurements of the wave velocities in shallow water.

3.2. Seismic Data

For seismic data we primarily use the three-component broadband seismometer VDOS operated by the Broadband Array in Taiwan for Seismology network located onshore of Pratas Island on the west side of Dongsha Atoll (Figure 1d). This Trillium 120-second posthole instrument is deployed near the ground surface at 2.7 meters depth and has a 100-Hz sampling rate. We additionally deployed two temporary broadband seismometers (6M88 and 6M75 on Figure 1d) on Pratas Island near the surface from May 11–June 4, 2019. The signal-to-noise ratio for these two instruments is lower than for VDOS; these stations are primarily used for confirmation of signals observed on VDOS.

Internal solitary waves of depression in the South China Sea propagate with velocities of 2–3.5 m/s (depending on water depth) and wavelengths of 1–2 km. Therefore, in the deep basin, the period of these waves is about 285–1,000 s. As the waves shoal at Dongsha Atoll, they slow and break up into a packet of shorter period (200–850 s) elevation waves (Davis et al., 2020; Fu et al., 2012). Therefore, it is reasonable to look for

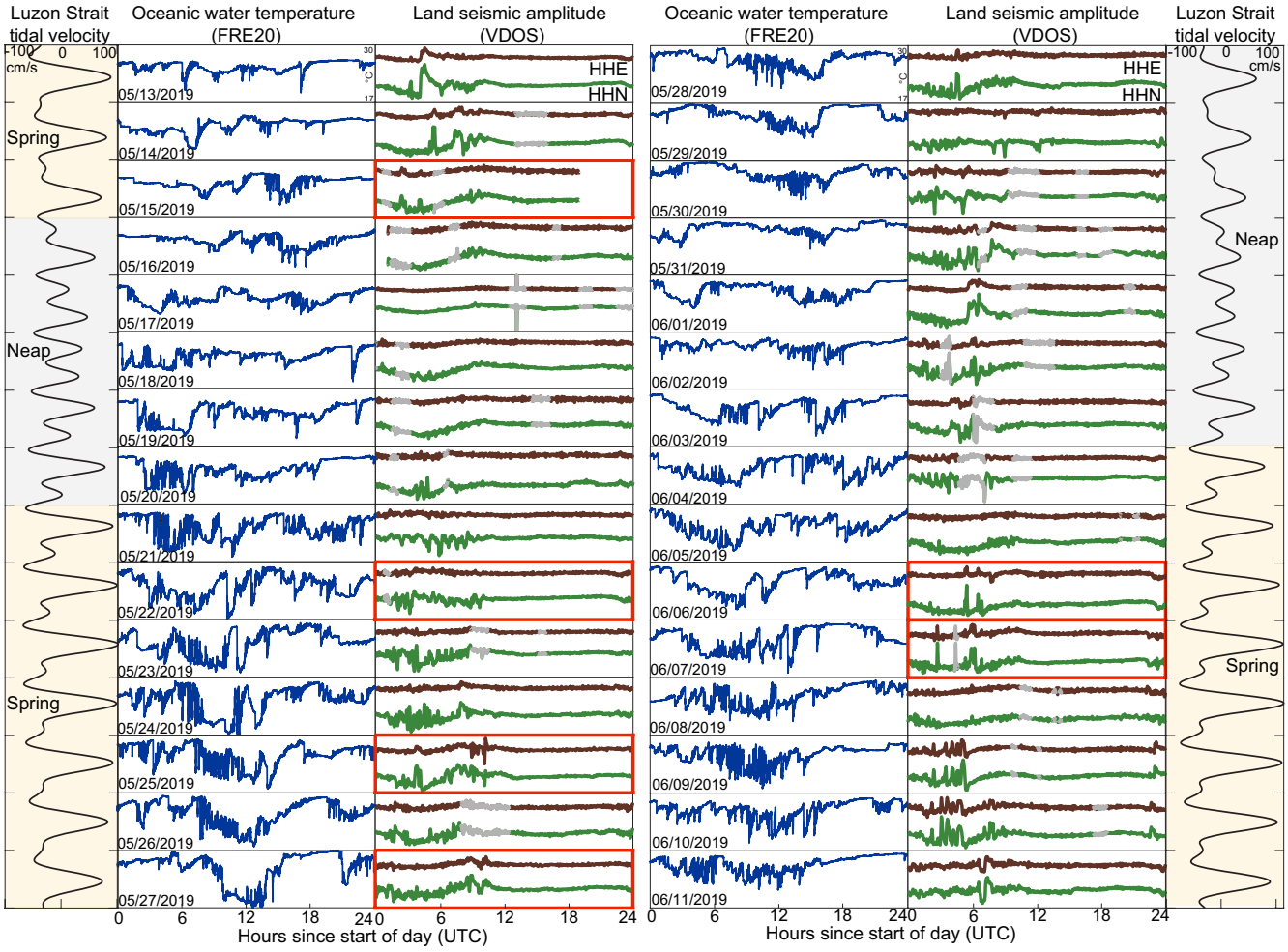

Figure 2. Oceanic water temperature and land seismic data from May 13–June 11, 2019. Oceanic water temperature measurements at 19 m depth from FRE20 (Figure 1d) on the east side of Dongsha Atoll are shown in blue. VDOS HHE (brown) and HHN (green) components are shown with an acausal 400-second low-pass filter applied. Earthquake time periods are highlighted in gray. The Luzon Strait tidal velocities (black lines) were estimated using the Oregon State Tidal Inversion Software (Egbert & Erofeeva, 2002) and plotted with a 50-hour time shift. Spring (yellow) and neap (gray) time periods are indicated. The days that the seismic data is analyzed in more detail in Sections 4.2–4.5 are highlighted in red.

a long period tilt signal of passing internal waves on the horizontal components of VDOS. We anticipate a seismically observable tilt signal within roughly 10 km of the source based on the 1–2 km wavelength of these waves. We first decimate the 100-Hz VDOS raw seismic data to 1 Hz by downsampling by a factor of 10 twice, each time applying a low-pass filter. We then apply an acausal (two-pass) 400-second low-pass filter to the decimated seismic data. We do not remove the instrument response when initially identifying small, transient tilt signals in VDOS that are potentially from internal wave activity to prevent identifying deconvolution artifacts as signals. The raw seismic data is in counts, which on VDOS is proportional to velocity at periods below 120 s.

There is a diurnal seismic tilt signal on the horizontal components of VDOS (Figure 2), 6M75 and 6M88 during daylight hours (22:00–10:00 UTC; 6 a.m.–6 p.m. local time). This presents a challenge in differentiating between other diurnal tilt-generating signals such as tidally modulated internal waves; the source of this diurnal tilt "noise" is therefore important. Daily temperature fluctuations can cause a change in instrument sensitivity at long periods. Daily temperature fluctuations for the tropical climate on Pratas Island are ~5°C (Figure S1). For this temperature change, the instrument sensitivity change is about 0.04% (Anthony et al., 2018). The diurnal tilt changes are greater than this sensitivity change. In addition, the Trillium 120-second posthole sensor is buried at 2.7 m depth, below the depth where surface temperature variations

are strongest. It is therefore unlikely that the diurnal tilt signal is from instrumental changes in sensitivity with temperature. It is more likely that the diurnal signal is from Pratas Island tilting as a result of diurnal temperature fluctuations as has been observed on other islands (Arnoso et al., 2001; Bilham & Beavan, 1979; Ekström et al., 2006). The amplitude variations of the seismic signal do not correlate with the amplitude of land temperature measurements recorded on the island (Figure S1). In particular, when daily temperature fluctuations on Pratas Island are largest (May 16–May 21), the diurnal tilt signal in the seismic recordings is lowest. However, the barometric pressure is larger at these time periods and may result in stronger thermal coupling. The north-south seismic components experience larger diurnal tilt signals than the east-west components; it is possible that Pratas Island preferentially tilts north-south due to its east-west elongation (Figure 1d). It is possible that the preferential north-south tilt Pratas Island will bias transient tilt signals in the north-south direction.

4. Observations

In order to find tilt signals on VDOS potentially generated by internal waves from the Luzon Strait we need to (a) identify transient tilt signals on VDOS, (b) compare the transient seismic tilt signals to established internal wave signals in satellite and oceanographic data, (c) verify that the tilt signals on VDOS are physical by comparing them to the temporary seismometers 6M75 and 6M88, and (d) determine whether tilt signals of interest are consistent with expected near-field tilt amplitudes generated by internal solitary waves in the South China Sea.

4.1. Transient Seismic Tilt Signals

There are transient increases in tilt within the longer period diurnal noise on VDOS HHN and HHE (Figure 2). These signals appear to be largest and most frequent during spring tide at the Luzon Strait (Figure 2) when the largest amplitude internal waves are generated. Further, transient seismic tilt signals appear to increase at times when the oceanic temperature record at FRE20 has the highest variance, indicative of internal wave activity (Davis et al., 2008) (Figure 2). It is therefore possible that some of the observed transient seismic tilt signals are due to internal waves arriving from the Luzon Strait. It should also be noted that the thermal transients on FRE20 are also due to non-tidal currents, the local internal tide, and locally generated internal waves, which may also generate tilt observable on VDOS.

4.2. Comparison of Seismic and Satellite Observations

We use the Himawari-8 geostationary satellite images on exceptionally clear days from June 6–7, 2019 (Figures 3a–3c; Movie S1) to identify internal waves on the western side of Dongsha Atoll for comparison to transient tilt signals on VDOS. We find that the largest transient increases in tilt on VDOS HHN and HHE are temporally correlated with times when internal waves are clearly visible on satellite images near the western side of Dongsha Atoll near Pratas Island and VDOS (Figures 3c and 4i; Movie S1). The potential seismic internal wave signals have durations of 30 min to 1 hour, are largest on the HHN component (Figures 3c and 4i), and are roughly 3.5–6 and 2–3 times the background noise on the HHN and HHE components, respectively (Figures S2 and S3). There appear to be two seismic internal wave signals on June 6 separated by 1 hour (Figure 3c). On June 7, there were two peaks in the transient tilt signal (Figure 4i) but there is little separation.

4.3. Comparison of Seismic and Oceanographic Observations

There was significant cloud cover from May 18–June 5, 2019 that prevented the detection of internal waves on satellite images. We can therefore only compare transient seismic tilt signals to thermal transients indicative of internal waves in oceanic water temperature data during this time period. However, differentiating between internal waves arriving from the Luzon Strait, the local internal tide, and locally generated internal waves at individual shallow oceanic temperature sensors is challenging, and all of these oceanic processes may generate tilt observable at VDOS. Further, depending on the depth of temperature measurements and the pycnocline, internal wave arrivals may be missed by individual shallow oceanic temperature sensors. We

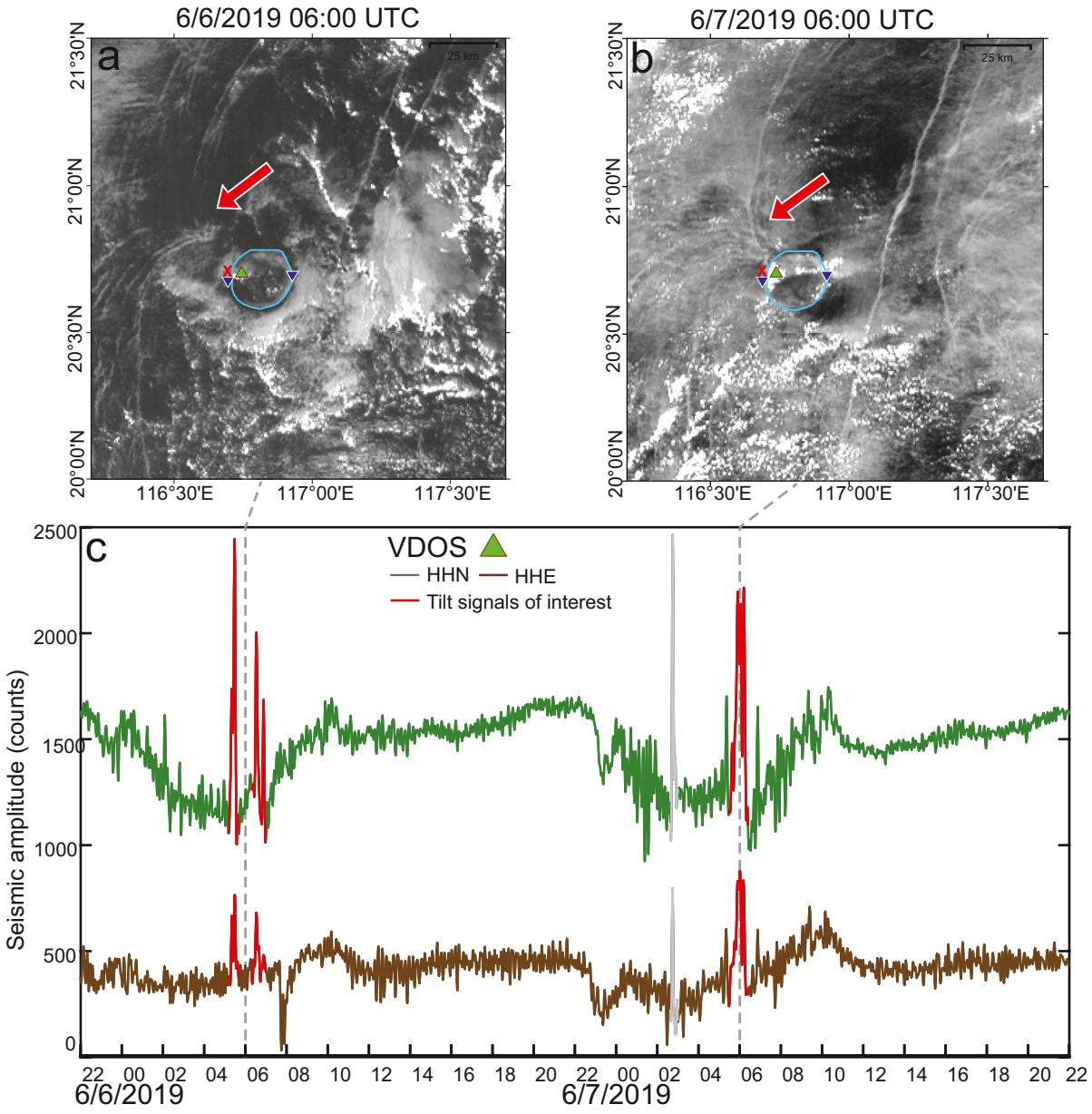

Figure 3. Comparison of satellite images and seismic observations as internal waves pass Dongsha Atoll. (a)–(b) Himawari-8 standard red channel images on June 6, 2019 06:00 UTC and June 7, 2019 06:00 UTC. Dongsha Atoll outlined in light blue. Seismic station VDOS on Pratas Island (green triangle) and oceanic temperature sensors (blue inverted triangles) are included. The closest point of internal waves to Pratas Island and VDOS is marked with a red X. Internal waves passing around the western side of Dongsha Atoll are indicated by the red arrows. (c) VDOS components HHE and HHN with an acausal 400-second low-pass filter applied. Tilt signals potentially correlating with timing of internal wave arrivals on the western side of Dongsha Atoll are indicated in red. Earthquake or instrument malfunction times are indicated in gray. The timing of the satellite images are indicated by the dashed gray lines. Time is in UTC. See Movie S1 for a movie of satellite images and seismic data from June 6–June 7, 2019.

therefore rely on the deeper oceanic moorings located 6–9 km east of FRE20 before waves interact strongly with the bottom as a guide of expected arrival times for internal waves generated at the Luzon Strait.

Guided by the deeper moorings we were able to identify internal wave arrivals from the Luzon Strait on May 25 (Figure 5b) and May 27, 2019 (Figure 5a) during spring tide at both the shallow oceanic water temperature sensors (FRE20 and FRW15), with arrivals at FRW15 lagging 2–4 h behind FRE20. There are clear transient seismic tilt signals of similar duration on VDOS HHN and HHE that lag 1–1.5 h behind FRW15 (Figures 5a and 5b). These lags are consistent with a packet of internal waves arriving at Dongsha Atoll from

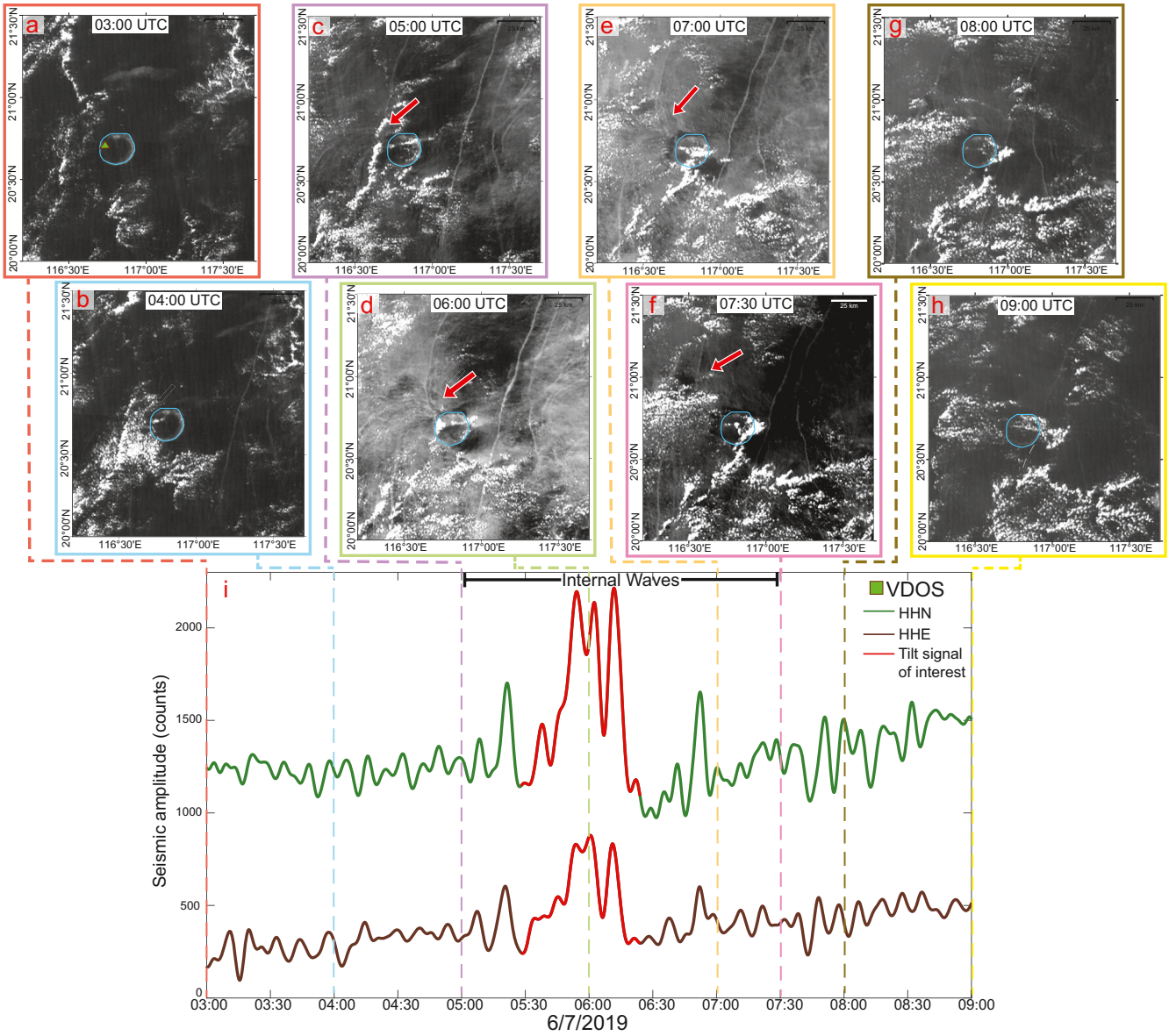

Figure 4. Detailed comparison of satellite images and seismic observations as internal waves pass Dongsha Atoll. (a–h) Himawari-8 standard red channel images on June 7, 2019 from 03:00–09:00 UTC. Dongsha Atoll is outlined in light blue. VDOS seismic station is shown as the green triangle on panel (a). Internal waves passing around the west side of Dongsha Atoll are indicated by the red arrows. (i) VDOS components HHE and HHN with an acausal 400-second low-pass filter applied. The largest tilt signal is highlighted in red. Timing of the satellite images are indicated with dashed lines corresponding to the border colors of the satellite images. The time period where internal waves are observed on the west side of Dongsha Atoll based on the satellite images is indicated. Time is in UTC. See Movie S1 for a movie of satellite images and seismic data from June 6–June 7, 2019.

the Luzon Strait, breaking into northern and southern arms as they refract around the atoll, with the southern arm passing FRW15 before reaching the nearest point to VDOS. We were additionally able to identify internal wave arrivals at FRE20 on May 22, 2019 during spring tide (Figure 5c). An internal wave signal is not clear on FRW15 at the anticipated arrival time; however, there are transient tilt signals in the seismic data near the expected arrival time (Figure 5c).

The thermal transient signals on FRE20 and FRW15 on May 25 and May 27 both related and potentially unrelated to internal wave activity warrant additional discussion. On May 27 the internal wave signal on FRW15 appears to occur during the local steepened internal tide. It is therefore possible that the observed seismic signal is from a combination of the internal wave arrival from the Luzon Strait and the local internal

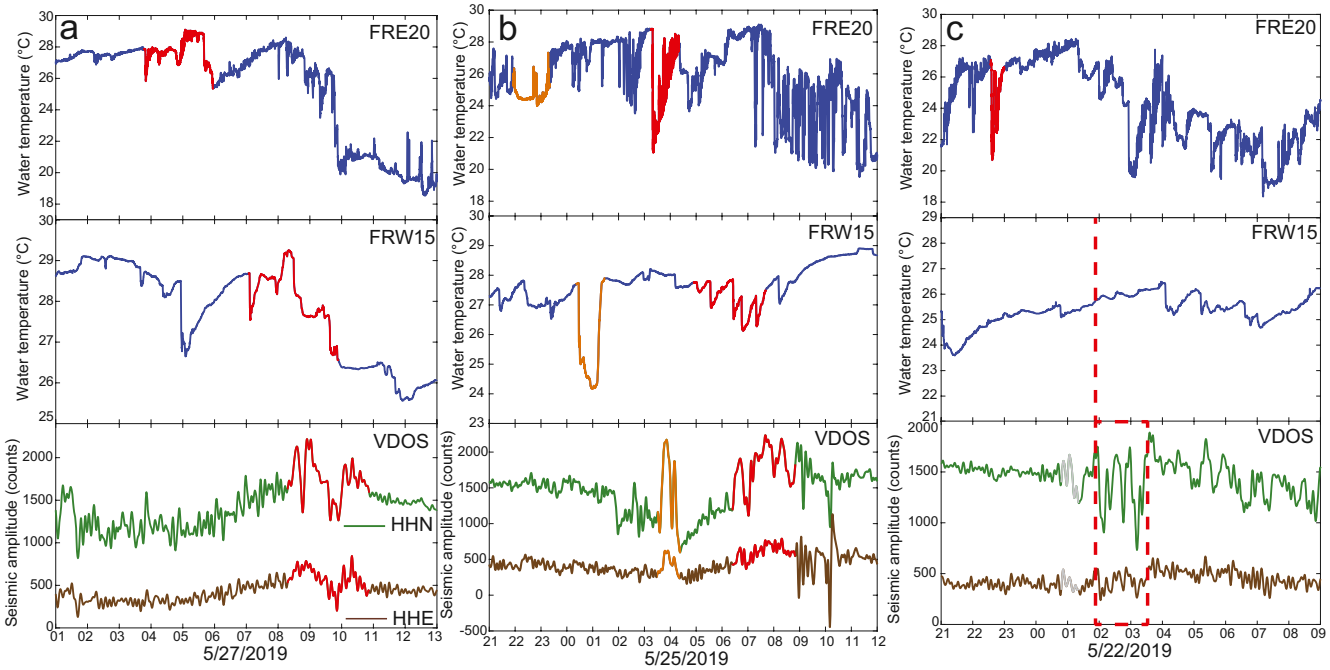

Figure 5. Comparison of shallow oceanic water temperature data to seismic observations at VDOS during spring tide on May 27 (a), May 25 (b), and May 22 (c). Top: Shallow water temperature measurements at 19 m depth (FRE20 on Figure 1d) on the east side of the Dongsha Atoll shown in blue. Middle: Shallow water temperature measurements on the ocean bottom at 16.8 m depth (FRW15 on Figure 1d) on the west side of Dongsha Atoll shown in blue. Bottom: VDOS components HHE (brown) and HHN (green) with an acausal 400-second low-pass filter applied. Internal wave signals arriving from the Luzon Strait on shallow temperature data and corresponding potential internal wave signals on VDOS are highlighted in red on (a and b). A potential local internal wave signal is highlighted in orange in (b). The approximate timing of internal wave arrivals on FRE20 is indicated by the red dashed line in (c) and a potential seismic signal is indicated by the red dashed box. Time is in UTC.

tide. Further, there was a temperature drop on FRW15 two hours prior to the internal wave arrival, which may also be related to the seismic signal (Figure 5a). On May 25 there was a large thermal transient propagating from FRE20 to FRW15 (highlighted in orange on Figure 5b) approximately 5 h prior to the internal wave arrival from the Luzon Strait. There is also a transient tilt signal on VDOS that is lagged 3 h behind FRW15. This lag is longer than the 1–1.5 hour lag observed for VDOS following FRW15 for internal wave arrivals from the Luzon Strait (Figures 5a and 5b). This signal was not observed at the deeper offshore moorings and is therefore unlikely to arrive from the Luzon Strait. This transient may instead be a locally generated internal wave. However, if this is an internal wave arrival from the Luzon Strait, the increased lag may be due to a collision point farther north of Pratas Island or a slower wave velocity.

4.4. Signal Across Seismic Stations

To verify that the transient tilt signals of interest on VDOS are physical, we select a time period (May 15, 2019) when two temporary seismometers (6M75 and 6M88) were operating and at least partial satellite identification of internal waves is available to corroborate the seismic signals. Internal waves are visible on satellite images on the west side of Dongsha Atoll at 05:40 UTC on May 15, 2019 (Figure 6b). However, internal waves have passed roughly 20 km west of Pratas Island by the time they can be clearly identified in the satellite image due to cloud cover. It is expected that transient tilt signals observed on broadband seismometers on Pratas Island would occur 3–5.5 h before this time depending on wave velocity ranging from 1–2 m/s. Two transient tilt signals are visible on VDOS, 6M75, and possibly on 6M88 (Figure 6a) starting around 02:00 and 04:00 UTC that are consistent with the satellite time constraints.

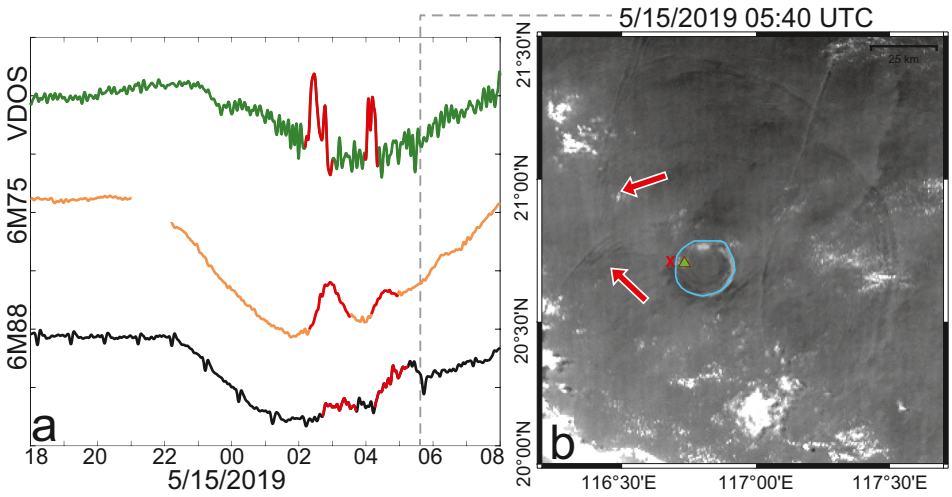

Figure 6. Comparison of tilt signal across seismic stations on May 15, 2019. (a) VDOS HHN (green), 6M75 BHN (orange), and 6M88 BHN (black) with acausal 400-second low-pass filters applied. Large transient tilt signals are highlighted in red. Timing of the satellite image in (b) is indicated by the gray dashed line. (b) Himawari-8 standard red channel images on May 15, 2019 at 05:40 UTC. Dongsha Atoll is outlined in blue. Seismic station VDOS on Pratas Island is indicated by the green triangle, the closest point of internal waves to Pratas Island and VDOS is marked with a red X. Internal waves that have recently passed Dongsha Atoll are indicated by the red arrows.

4.5. Seismic Amplitude

We can estimate the seismic amplitudes during the 6 days of potential internal wave arrivals detailed in Sections 4.1–4.4. We first deconvolve the instrument response to acceleration. We performed a simple linear detrend and then applied a cosine taper band-pass filter with four corner frequencies appropriate for identifying long-period tilt signals expected from internal waves (1/2,400 Hz, 1/1,200 Hz, 0.5 Hz, and 1 Hz). After the response was deconvolved we decimated the 100-Hz data to 1 Hz by downsampling by a factor of 10 twice, each time applying a low-pass filter. We then applied an acausal 400-second low-pass filter to the seismic data and analyzed the previously identified potential seismic internal wave signals in the raw seismic data (Figure 7). It appears that peak seismic tilt signals range from roughly 35–80 nrad on VDOS HHN (Figure 7). Tilt amplitudes are smaller for VDOS HHE, ranging from 15 to 35 nrad.

5. Summary of Observations and Potential Mechanisms

We have found promising evidence of the seismic detection of internal waves. First, there are transient tilt signals on a permanent broadband seismometer onshore of Pratas Island that appear to be larger and occur more frequently during spring tide when the largest amplitude internal waves in the South China Sea are generated at the Luzon Strait (Figure 2). These are also the time periods when the oceanographic temperature records have the highest variance, indicative of internal wave activity (Davis et al., 2008). Second, we were able to temporally correlate some of these transient seismic tilt signals with internal wave detections near Pratas Island from satellite and oceanic water temperature measurements (Figures 3–6). Third, some of the transient seismic tilt signals that correlate temporally with satellite and oceanographic measurements are also observed on temporary seismometers on Pratas Island, indicating that these tilt signals are physical (Figure 6). Finally, the seismic amplitude of the tilt signals of interest are on the order of tens of nrad, consistent with expectations for a near-field elastic tilt signal generated by internal solitary waves in the South China Sea (see Text S2 for calculation) (Figure 7). These observations taken together are strong evidence of the seismic detection of internal waves.

We now consider two mechanisms to generate seismically observable transient tilt signals through the pressure coupling of internal waves with the underlying seafloor.

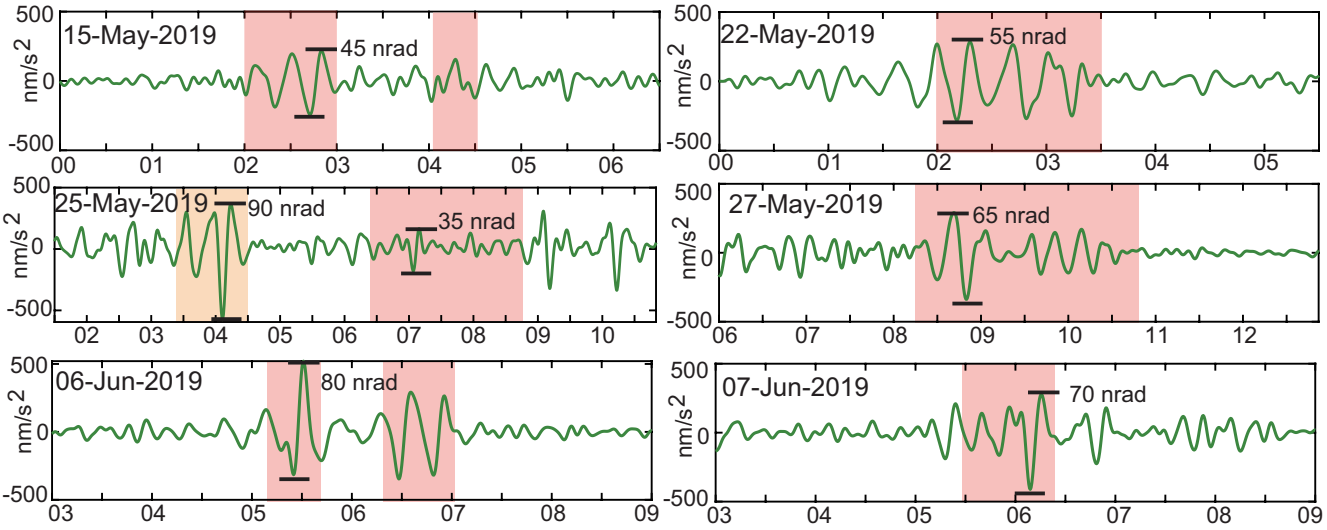

Figure 7. Amplitude of seismic internal wave detections. VDOS HHN (green) with the response deconvolved and an acausal 400-second low-pass filter. Approximate timing of internal waves near Pratas Island arriving from the Luzon Strait highlighted in red. A potential local internal wave signal on May 25 highlighted in orange. Rough peak tilt amplitudes in nanoradians during internal wave time periods indicated in black. Timing (in hours) is UTC.

5.1. Passing of Internal Waves

The most straightforward mechanism for an internal wave to generate a seismically observable transient tilt signal is simply by passing near a broadband seismometer. As discussed in Section 1, the hydrostatic pressure change and resulting elastic deformation of the underlying seafloor from a propagating internal solitary wave typical in the South China Sea would cause a near-field tilt of around 40 nrad (Figure 1a; Text S2). This is a useful conceptual framework, though it is oversimplified for the geometry of Dongsha Atoll and requires further discussion.

Internal waves arriving from the Luzon Strait refract around Dongsha Atoll. Therefore, the nearest point internal waves reach to VDOS on Pratas Island is at the fore reef approximately 4 km west of VDOS (marked on Figure 3a). It is anticipated that the largest hydrostatic pressure change and therefore near-field tilt signal observable by VDOS would occur at this point. This would generate a smaller tilt signal than expected from our calculation (Text S2), which assumes the wave directly passes the seismometer. In addition, the waves are broken into a packet of elevation waves, rather than a single solitary wave of depression, which would further complicate the expected tilt signal.

It is worth noting that the two peaks in transient tilt observed on VDOS on June 6 (Figure 3c) are consistent with the deeper mooring observation that this arrived as a two-packet wave. The June 7 wave was a single solitary wave and only one primary peak was observed in the seismic data (Figure 3c).

5.2. Collision of Internal Waves

Another mechanism for internal waves to generate near-field tilt signals large enough to be observed seismically is from wave-wave interactions or collisions. This is because breaking or interacting internal waves can produce dynamic pressure changes on the seafloor in addition to hydrostatic pressure changes expected from a passing wave (Moum & Smyth, 2006). The dynamics of nonlinear internal wave interactions are complex and dependent upon the wave amplitudes and interaction angle (Wang & Pawlowicz, 2012). While our measurements do not permit a detailed characterization of the interaction region, satellite imagery of the Dongsha Atoll region clearly shows that as a soliton propagates past the shallow bathymetry of the atoll, it breaks into northern and southern arms that collide after reaching the west side of Dongsha Atoll before eventually reforming (Hsu & Liu, 2000; Li et al., 2013) (Figures 1c, 3a, 3b, and 4c–4f, Movie S1). These nonlinear wave-wave interactions would generate both dynamic and hydrostatic pressure changes coupled

to the seafloor, causing near-field elastic displacement and tilt that are expected to be larger and thus more observable than for a single propagating wave. We favor this mechanism for several reasons.

First, the observed tilt signals on the north-south component of VDOS range from 35–80 nrad (Figure 7). This is larger than the 40 nrad expected from the hydrostatic pressure change alone, although it is still within the error of this simple calculation. Second, the seismic tilt signals lag 1–2 h behind internal wave detections on the nearest oceanic temperature sensor (FRW15). The point of nearest approach to VDOS is roughly 3 km north of FRW15; we therefore expect internal waves to first be detected on FRW15. However, considering wave velocities ranging from 0.5–2 m/s, the seismic tilt signals are anticipated to lag 25–100 min behind FRW15. The larger observed lag suggests that the peak seismic tilt signals are generated after the waves pass the nearest point to VDOS, potentially when the northern and southern arms interact. The seismic signal from wave-wave interactions may be from the collisions of multiple waves within a packet at the crossover point of the northern and southern arms. Based on satellite images during the study period (Figures 3a, 3b, and 4c–4f, Movie S1), these collisions occur north-northwest of Pratas Island, within the expected observational limit of VDOS of roughly 10 km.

6. Caveats and Conundrums

6.1. North-South Dominant Tilt

The likely internal wave signals on VDOS are largest on the north-south component. This may be due to a combination of the preferential tilt of the island as well as the source of the tilt signals. It is likely that the east-west elongated Pratas Island preferentially tilts north-south, as is observed with the diurnal tilt signal (Figures 2 and S1). It is unclear at this point if the preferential north-south tilt of Pratas Island would create a north-south bias for other transient tilt sources. In addition, internal waves "wrap" north-south around Dongsha Atoll (Li et al., 2013). When the northern and southern arms meet and collide on the west side of Dongsha Atoll, they are still propagating in a north-south direction (Figures 3a, 3b, and 4c–4f). This may produce a dominant north-south tilt. Further, the tilt experienced on Pratas Island may be amplified if this collision point occurs farther north or south, rather than due west of the island.

6.2. Detection of Only One Type of Wave

During the study period all the potential internal wave signals identified in the seismic data occur between 02:00 and 11:00 UTC (10:00 and 19:00 local time). This is predominantly during daylight hours and within the large diurnal seismic tilt noise. No potential internal wave detections are made more than once per day. However, internal waves are generated up to twice daily at the Luzon Strait and have been classified as type-a or type-b waves (Duda et al., 2004; Ramp et al., 2004). Type-a waves are generated primarily by the K1 tide, typically have a large amplitude wave followed by smaller amplitude waves, and arrive at the same time each day, 24 h apart (Duda et al., 2004; Ramp et al., 2004). Type-b waves have a larger contribution from the M2 tidal constituent, propagate as a packet of waves, and arrive approximately one hour later each day (Duda et al., 2004; Ramp et al., 2004). Type-b waves are generated in the northern portion of the Luzon Strait while type-a waves are generated farther south (Du et al., 2008; Ramp et al., 2019). The deeper moorings provide more detailed observations of type-a and type-b waves during the deployment period. In general, type-a waves arrived as two or three-wave packets at an angle more south of east. Type-b waves arrived from almost due east as solitary waves that then broke into multi-wave packets of approximately equal amplitude and spacing between waves.

All of the potential seismic signals we identify are from type-b waves. During the study period, type-b waves arrive on the west side of Dongsha Atoll during daylight hours which allows for identification of these waves and wave-wave interactions on clear days near Pratas Island using satellite imagery. Type-a waves arrive at the east side of Dongsha Atoll around 09:00 UTC (17:00 local time). We can therefore at times identify their arrival but cannot track these waves to the west side for better temporal comparison to onshore seismic data. This makes identifying a seismic signal from type-a waves difficult. Still, there are no clear transient tilt signals on VDOS during expected type-a arrival times on the west side of Dongsha Atoll. Below is a discussion of why type-a waves, and some type-b waves, may not be detected by VDOS.

The collision of the northern and southern arms refracting around Dongsha Atoll is likely a key generator of seismically observable tilt (see Section 5.2). Therefore, refraction of waves around Dongsha Atoll and the location of the western collision are important for tilt generation. It is thus potentially significant that in this study only type-b waves have been observed to refract around Dongsha Atoll. This may be due to lack of satellite observations of type-a waves, or lack of satellite signature of type-a waves refracting.

Potential reasons for type-b waves to generate a seismically observable tilt while type-a waves do not include systematic differences in incoming angle, frequency content, depth of the main thermocline upon arrival during local internal tide, or interactions with the bottom. For instance, empirically it is seen that type-b waves refract asymmetrically around Dongsha Atoll resulting in the western collision occurring north-northwest of Pratas Island (Figures 3a, 3b, and 4c–4f, Movie S1). This may be due to the incoming angle, bathymetry and bathymetry-related velocity differences around the atoll. This asymmetry can generate a larger north-south pressure change and therefore north-south tilt of the underlying seafloor. Since the east-west elongated Pratas Island likely preferentially tilts north-south, this may be a more observable signal. Alternatively, type-a waves arrived with the local tide, creating more disturbances in the thermocline. Last and more speculatively, type-a and type-b waves may interact differently in the near-shore environment due to their frequency content. Type-a and type-b waves are generated in different parts of the Luzon Strait (Du et al., 2008; Ramp et al., 2019). This difference in generation site may affect the frequency content of the waves which may ultimately impact the interactions in the near-shore environment observed in the seismic data.

Not all type-b waves are clearly detected in the seismic data above the noise. The amplitude of waves will also determine the pressure change and near-field tilt signal. The diurnal tilt noise is around 5–10 nrad. Therefore, the tilt signal from a relatively small amplitude internal wave, potentially during neap tide, can likely be hidden in the diurnal tilt noise.

6.3. Seismic Performance Compared to Existing Methods

There are transient tilt signals on VDOS throughout the study period that we have not correlated with internal waves arriving from the Luzon Strait. This is partially due to incomplete satellite and oceanographic measurement coverage; however, it is likely that some of these signals are not from internal waves generated at the Luzon Strait. The local internal tide and locally generated internal waves may also cause observable transient tilt signals on VDOS. Caution is therefore warranted at this time when identifying internal wave signals and their origin using seismic data alone.

Satellite imagery can provide remarkable spatial detail and identification of internal waves. However, satellite visible images are limited temporally, are unavailable at night and are highly unreliable during daylight hours. The deeper oceanic temperature moorings reliably detect internal waves of depression before they have interacted with the bottom and transformed, but are limited spatially. The shallow oceanic temperature sensors record internal waves after they have transformed into packets of elevation waves and are shoaling or breaking in the near-shore environment. The shallow temperature sensors are noisy, recording complicated near-shore internal wave interactions as well as non-tidal currents, the local internal tide, and locally generated internal waves. Other measurements, such as satellite images or deeper moorings, are required to reliably identify internal waves arriving from the Luzon Strait in the shallow temperature data. The seismic data also requires additional verification of internal wave identification at this time, but is currently performing similarly to the shallow temperature sensors. This work is a first proof of concept using onshore seismometers to detect internal waves. Necessarily, the proof of concept is being done where independent data demonstrating the existence of the waves is available. The logical next step would be to utilize the seismic data to identify waves in the absence of such ground truth and we hope to achieve that in future work.

6.4. Mechanism

As discussed in Section 5, the mechanism for internal waves to generate seismically observable tilt signals on Pratas Island is unclear. However, we favor large (i.e., observable by VDOS) transient tilt signals generated on the west side of Dongsha Atoll near Pratas Island as the northern and southern arms collide and

reform, generating both hydrostatic and dynamic pressure changes on the underlying seafloor and therefore near-field displacement and tilt.

7. Conclusion

It appears that we have successfully detected oceanic internal waves using a subaerial island seismometer for the first time. We observe dominant north-south transient tilt signals on a broadband seismic station onshore of Pratas Island with amplitudes similar to what is expected from internal solitary waves arriving from the Luzon Strait. These seismic tilt signals appear correlated with internal wave detections in satellite and oceanic data, and apparently occur when waves collide nearshore. The north-south dominance is consistent with internal waves refracting around Dongsha Atoll and the east-west elongated Pratas Island preferentially tilting north-south. This initial detection suggests that the onshore seismic detection and amplitude determination of oceanic internal waves is possible and can potentially be used to expand the historical record by capitalizing on existing island and coastal seismic stations.

Conflict of Interest

The authors declare no conflicts of interest relevant to this study.

Data Availability Statement

Maps were produced with the Generic Mapping Tools. Waveform data from the permanent seismic station used in this study are available at the Broadband Array in Taiwan for Seismology, Institute of Earth Sciences, Academia Sinica, Taiwan (doi: 10.7914/SN/TW). Waveform data from the temporary onshore deployment are archived at the Incorporated Research Institutions for Seismology Data Management Center (doi: 10.7914/SN/YD_2019). Land temperature, humidity, and barometric pressure data from the temporary onshore deployment are archived at PANGAEA (doi: 10.1594/PANGAEA.931741). The shallow oceanic temperature data are archived at Dryad (doi: 10.7280/D1S39W). Satellite data is from the Himawari-8 geostationary meteorological satellite operated by the Japan Meteorological Agency.

Acknowledgments
We are grateful for the support of Dongsha Atoll Research Station and Dongsha Atoll Marine National Park. We are further grateful to Keryea Soong, Yi-Bei Liang, and Ke-Hsien Fu at National Sun Yat-sen University, Taiwan, and to Greg Sinnett and Sarah Merrigan, for their efforts in making this research possible. We are very grateful to Prof. Kuo-Fong Ma at Institute of Earth Sciences, Academia Sinica and National Central University in Taiwan for help accessing the VDOS seismic data and Profs. Sen Jan, Y. J. Yang, and Ming-Huei Chang at National Taiwan University for the use of their deep mooring data for this study. The authors would also like to thank Thorne Lay for informative discussions that improved this work. K.A.D. was supported through funding provided by NSF-OCE 1753317.

References

Ackerley, N. (2014). Principles of broadband seismometry. In M. Beer, I. A. Kougioumtzoglou, E. Patelli, & I. S.-K. Au (Eds.), *Encyclopedia of earthquake engineering* (pp. 1–35). Berlin, Heidelberg. Springer Berlin Heidelberg. https://doi.org/10.1007/978-3-642-36197-5_172-1

Alford, M. H., Peacock, T., MacKinnon, J. A., Nash, J. D., Buijsman, M. C., Centurioni, L. R., et al. (2015). The formation and fate of internal waves in the South China Sea. *Nature*, *521*, 65–69. https://doi.org/10.1038/nature14399

Alpers, W. (1985). Theory of radar imaging of internal waves. *Nature*, *314*, 245–247. https://doi.org/10.1038/314245a0

Anthony, R. E., Ringler, A. T., & Wilson, D. C. (2018). Improvements in Absolute Seismometer Sensitivity Calibration Using Local Earth Gravity Measurements Short Note. *Bulletin of the Seismological Society of America*, *108*, 503–510. https://doi.org/10.1785/0120170218

Arnoso, J., Viera, R., Velez, E., Weixin, C., Shiling, T., Jun, J., & Venedikov, A. (2001). Monitoring tidal and non-tidal tilt variations in Lanzarote Island (Spain). *Journal of the Geodetic Society of Japan*, *47*, 456–462. https://doi.org/10.11366/sokuchi1954.47.456

Bilham, R., & Beavan, J. (1979). *Surface deformation and elasticity studies in the Virgin Islands* (Vol. 5072). National Aeronaautics and Space Administration NSG.

Boudin, F., Allgeyer, S., Bernard, P., Hébert, H., Olcay, M., Madariaga, R., et al. (2013). Analysis and modelling of tsunami-induced tilt for the 2007, M = 7.6, Tocopilla and the 2010, M = 8.8 Maule earthquakes, Chile, from long-base tiltmeter and broadband seismometer records. *Geophysical Journal International*, *194*(1), 269–288. https://doi.org/10.1093/gji/ggt123

Bromirski, P. D. (2001). Vibrations from the "perfect storm". *Geochemistry, Geophysics, Geosystems*, *2*(7), 1030. https://doi.org/10.1029/2000GC000119

Bromirski, P. D., Duennebier, F. K., & Stephen, R. A. (2005). Mid-ocean microseisms. *Geochemistry, Geophysics, Geosystems*, *6*(4), Q04009. https://doi.org/10.1029/2004GC000768

Chang, E. T. Y., Chao, B. F., Chen, G.-Y., & Liau, J.-M. (2016). Internal tides recorded at ocean bottom off the coast of Southeast Taiwan. *Journal of Geophysical Research: Oceans*, *121*(5), 3381–3394. https://doi.org/10.1002/2015JC011370

Davis, K. A., Arthur, R. S., Reid, E. C., Rogers, J. S., Fringer, O. B., DeCarlo, T. M., & Cohen, A. L. (2020). Fate of Internal Waves on a Shallow Shelf. *Journal of Geophysical Research: Oceans*, *125*, e2019JC015377. https://doi.org/10.1029/2019JC015377

Davis, K. A., Leichter, J. J., Hench, J. L., & Monismith, S. G. (2008). Effects of western boundary current dynamics on the internal wave field of the Southeast Florida shelf. *Journal of Geophysical Research*, *113*, C09010. https://doi.org/10.1029/2007JC004699

DeCarlo, T. M., Karnauskas, K. B., Davis, K. A., & Wong, G. T. F. (2015). Climate modulates internal wave activity in the Northern South China Sea. *Geophysical Research Letters*, *42*, 831–838. https://doi.org/10.1002/2014GL062522

Dolenc, D., Romanowicz, B., McGill, P., & Wilcock, W. (2008). Observations of infragravity waves at the ocean-bottom broadband seismic stations Endeavour (KEBB) and Explorer (KXBB). *Geochemistry, Geophysics, Geosystems*, *9*(5), Q05007. https://doi.org/10.1029/2008GC001942

Du, T., Tseng, Y.-H., & Yan, X.-H. (2008). Impacts of tidal currents and Kuroshio intrusion on the generation of nonlinear internal waves in Luzon Strait. *Journal of Geophysical Research*, *113*, C08015. https://doi.org/10.1029/2007JC004294

Duda, T. F., Lynch, J. F., Irish, J. D., Beardsley, R. C., Ramp, S. R., Chiu, C.-S., et al. (2004). Internal tide and nonlinear internal wave behavior at the continental slope in the northern South China Sea. *IEEE Journal of Oceanic Engineering*, *29*, 1105–1130. https://doi.org/10.1109/JOE.2004.836998

Egbert, G. D., & Erofeeva, S. Y. (2002). Efficient inverse modeling of barotropic ocean tides. *Journal of Atmospheric and Oceanic Technology*, *19*, 183–204. https://doi.org/10.1175/1520-0426(2002)019<0183:EIMOBO>2.0.CO;2

Ekström, G., Dalton, C. A., & Nettles, M. (2006). Observations of time-dependent errors in long-period instrument gain at global seismic stations. *Seismological Research Letters*, *77*, 12–22. https://doi.org/10.1785/gssrl.77.1.12

Ferrari, R., & Wunsch, C. (2009). Ocean circulation kinetic energy: Reservoirs, sources, and sinks. *Annual Review of Fluid Mechanics*, *41*, 253–282. https://doi.org/10.1146/annurev.fluid.40.111406.102139

Fu, K.-H., Wang, Y.-H., St. Laurent, L., Simmons, H., & Wang, D.-P. (2012). Shoaling of large-amplitude nonlinear internal waves at Dongsha Atoll in the northern South China Sea. *Continental Shelf Research*, *37*, 1–7. https://doi.org/10.1016/j.csr.2012.01.010

Fukao, Y., Sugioka, H., Ito, A., Shiobara, H., Paros, J. M., & Furue, R. (2016). Sensing of upslope passages of frontal bores across the trench slope break of the Japan Trench. *Journal of Geophysical Research: Oceans*, *121*(5), 3422–3434. https://doi.org/10.1002/2015JC011432

Garrett, C., & Kunze, E. (2007). Internal tide generation in the deep ocean. *Annual Review of Fluid Mechanics*, *39*, 57–87. https://doi.org/10.1146/annurev.fluid.39.050905.110227

Helfrich, K. R., & Melville, W. K. (2006). Long nonlinear internal waves. *Annual Review of Fluid Mechanics*, *38*, 395–425. https://doi.org/10.1146/annurev.fluid.38.050304.092129

Holloway, P. E., Pelinovsky, E., Talipova, T., & Barnes, B. (1997). A nonlinear model of internal tide transformation on the Australian North West Shelf. *Journal of Physical Oceanography*, *27*, 26. https://doi.org/10.1175/1520-0485(1997)027<0871:anmoit>2.0.co;2

Hsu, M.-K., & Liu, A. K. (2000). Nonlinear internal waves in the South China Sea. *Canadian Journal of Remote Sensing*, *26*(2), 72–81. https://doi.org/10.1080/07038992.2000.10874757

Jackson, C., da Silva, J., Jeans, G., Alpers, W., & Caruso, M. (2013). Nonlinear internal waves in synthetic aperture radar imagery. *Oceanography*, *26*, 68–79. https://doi.org/10.5670/oceanog.2013.32

Li, X., Jackson, C. R., & Pichel, W. G. (2013). Internal solitary wave refraction at Dongsha Atoll, South China Sea. *Geophysical Research Letters*, *40*, 3128–3132. https://doi.org/10.1002/grl.50614

Lien, R.-C., Tang, T. Y., Chang, M. H., & D'Asaro, E. A. (2005). Energy of nonlinear internal waves in the South China Sea. *Geophysical Research Letters*, *32*, L05615. https://doi.org/10.1029/2004GL022012

Lindsey, N. J., Dawe, T. C., & Ajo-Franklin, J. B. (2019). Illuminating seafloor faults and ocean dynamics with dark fiber distributed acoustic sensing. *Science*, *366*(6469), 1103–1107. https://doi.org/10.1126/science.aay5881

MacKinnon, J. A., Zhao, Z., Whalen, C. B., Waterhouse, A. F., Trossman, D. S., Sun, O. M., et al. (2017). Climate process team on internal wave–driven ocean mixing. *Bulletin of the American Meteorological Society*, *98*, 2429–2454. https://doi.org/10.1175/BAMS-D-16-0030.1

Miropol'sky, Y. Z. (2001). In O. D. Shishkina (Ed.), *Dynamics of internal gravity waves in the ocean*. Springer Netherlands, Atmospheric and Oceanographic Sciences Library. https://www.springer.com/us/book/9780792369356

Moum, J. N., & Smyth, W. D. (2006). The pressure disturbance of a nonlinear internal wave train. *Journal of Fluid Mechanics*, *558*, 153. https://doi.org/10.1017/S0022112006000036

Munk, W., Zetler, B., Clark, J., Glll, S., Porter, D., Spiesberger, J., & Spindel, R. (1981). Tidal effects on long-range sound transmission. *Journal of Geophysical Research*, *86*(C7), 6399–6410. https://doi.org/10.1029/JC086iC07p06399

Nawa, K., Suda, N., Satake, K., Fujii, Y., Sato, T., Doi, K., et al. (2007). Loading and gravitational effects of the 2004 Indian Ocean Tsunami at Syowa Station, Antarctica. *Bulletin of the Seismological Society of America*, *97*(1A), S271–S278. https://doi.org/10.1785/0120050625

Nishida, K., Maeda, T., & Fukao, Y. (2019). Seismic observation of tsunami at island broadband stations. *Journal of Geophysical Research: Solid Earth*, *124*(2), 1910–1928. https://doi.org/10.1029/2018JB016833

Orcutt, J. A., Cox, C. S., Kibblewhite, A. C., Kuperman, W. A., & Schmidt, H. (1993). Observations and causes of ocean and seafloor noise at ultra-low and very-low frequencies. In B. R. Kerman (Ed.), *Natural physical sources of underwater sound: Sea surface sound (2)* (pp. 203–232). Dordrecht. Springer Netherlands. https://doi.org/10.1007/978-94-011-1626-8_17

Ramp, S. R., Park, J.-H., Yang, Y. J., Bahr, F. L., & Jeon, C. (2019). Latitudinal structure of solitons in the South China Sea. *Journal of Physical Oceanography*, *49*, 1747–1767. https://doi.org/10.1175/JPO-D-18-0071.1

Ramp, S. R., Tang, T. Y., Duda, T. F., Lynch, J. F., Liu, A. K., Chiu, C.-S., et al. (2004). Internal solitons in the northeastern South China Sea. Part I: Sources and deep water propagation. *IEEE Journal of Oceanic Engineering*, *29*, 1157–1181. https://doi.org/10.1109/JOE.2004.840839

Ramp, S. R., Yang, Y. J., & Bahr, F. L. (2010). Characterizing the nonlinear internal wave climate in the northeastern South China Sea. *Nonlinear Processes in Geophysics*, *17*, 481–498. https://doi.org/10.5194/npg-17-481-2010

Ray, R. D., & Mitchum, G. T. (1996). Surface manifestation of internal tides generated near Hawaii. *Geophysical Research Letters*, *23*, 2101–2104. https://doi.org/10.1029/96GL02050

Reid, E. C., DeCarlo, T. M., Cohen, A. L., Wong, G. T. F., Lentz, S. J., Safaie, A., et al. (2019). Internal waves influence the thermal and nutrient environment on a shallow coral reef. *Limnology & Oceanography*, *64*, 1949–1965. https://doi.org/10.1002/lno.11162

Rogers, J. S., Rayson, M. D., Ko, D. S., Winters, K. B., & Fringer, O. B. (2019). A framework for seamless one-way nesting of internal wave-resolving ocean models. *Ocean Modelling*, *143*, 101462. https://doi.org/10.1016/j.ocemod.2019.101462

Sandstrom, H., & Elliott, J. A. (1984). Internal tide and solitons on the Scotian Shelf: A nutrient pump at work. *Journal of Geophysical Research*, *89*, 6415–6426. https://doi.org/10.1029/JC089iC04p06415

Simmons, H., Chang, M.-H., Chang, Y.-T., Chao, S.-Y., Fringer, O., Jackson, C., & Ko, D. S. (2011). Modeling and Prediction of internal waves in the South China Sea. *Oceanography*, *24*, 88–99. https://doi.org/10.5670/oceanog.2011.97

Sugioka, H., Fukao, Y., & Hibiya, T. (2005). Submarine volcanic activity, ocean-acoustic waves and internal ocean tides. *Geophysical Research Letters*, *32*(24), L24616. https://doi.org/10.1029/2005GL024001

Tanimoto, T. (2007). Excitation of microseisms. *Geophysical Research Letters*, *34*(5), L05308. https://doi.org/10.1029/2006GL029046

Wang, C., & Pawlowicz, R. (2012). Oblique wave-wave interactions of nonlinear near-surface internal waves in the Strait of Georgia. *Journal of Geophysical Research*, *117*(C6), C06031. https://doi.org/10.1029/2012JC008022

Wang, Y.-H., Dai, C.-F., & Chen, Y.-Y. (2007). Physical and ecological processes of internal waves on an isolated reef ecosystem in the South China Sea. *Geophysical Research Letters*, *34*, L18609. https://doi.org/10.1029/2007GL030658

Wielandt, E., & Forbriger, T. (1999). Near-field seismic displacement and tilt associated with the explosive activity of Stromboli. *Annals of Geophysics*, *42*. https://doi.org/10.4401/ag-3723

Wolanski, E., & Deleersnijder, E. (1998). Island-generated internal waves at Scott Reef, Western Australia. *Continental Shelf Research*, *18*, 1649–1666. https://doi.org/10.1016/S0278-4343(98)00069-7

Woodson, C. B. (2018). The fate and impact of internal waves in nearshore ecosystems. *Annual Review of Marine Science*, *10*, 421–441. https://doi.org/10.1146/annurev-marine-121916-063619

Wu, W., Zhan, Z., Peng, S., Ni, S., & Callies, J. (2020). Seismic ocean thermometry. *Science*, *369*(6510), 1510–1515. https://doi.org/10.1126/science.abb9519

Yuan, X., Kind, R., & Pedersen, H. A. (2005). Seismic monitoring of the Indian Ocean tsunami. *Geophysical Research Letters*, *32*(15), L15308. https://doi.org/10.1029/2005GL023464

Zhao, Z., Klemas, V., Zheng, Q., & Yan, X.-H. (2004). Remote sensing evidence for baroclinic tide origin of internal solitary waves in the northeastern South China Sea. *Geophysical Research Letters*, *31*, L06302. https://doi.org/10.1029/2003GL019077